Supporting information

Interplay between Spin-Crossover and Luminescence in a Multifunctional Single Crystal Iron (II) complex: Towards a New Generation of Molecular Sensors

Bouabdellah Benaicha,[a] Khanh Van Do,[b] Aymen Yangui,[c] Narsimhulu Pittala,[a] Alain Lusson,[b] Mouhamadou Sy,[b] Guillaume Bouchez,[b] Houcem Fourati,[b] Carlos J. Gómez-García,[d] Smail Triki,[a] and Kamel Boukheddaden[b*]*

[a.] *Univ Brest, CNRS, CEMCA, 6 Avenue Victor Le Gorgeu, C.S. 93837 - 29238 Brest Cedex 3, France. Email : Smail.Triki@univ-brest.fr*

[b.] *Groupe d'Etude de la Matière Condensée, CNRS UMR8635, Université de Versailles Saint Quentin, Université Paris-Saclay, 45 avenue des Etats-Unis, 78035 Versailles cedex, France Email : Kamel.boukheddaden@uvsq.fr.*

[c.] *Department of Chemistry and Biochemistry, University of Oklahoma, 101 Stephenson Parkway, Norman, OK 73019, USA.*

[d.] *Instituto de Ciencia Molecular (ICMol). Departamento de Química Inorgánica. Universidad de Valencia. C/Catedrático José Beltrán 2. 46980 Paterna, Spain.*

Table of Contents

1 - Syntheses

1.1 - General experimental procedure:

All the starting reagents were purchased from commercial sources (Sigma-Aldrich, Across, Fisher Scientific, Alfa Aesar and Merck) and used as received. Solvents were dried by refluxing under nitrogen over the appropriate drying agents (calcium hydride for acetonitrile, dichloromethane, and hexane; magnesium and iodine for methanol; sodium for ethanol, and molecular sieves for DMF), and then degassed before use. Solvents were also obtained from a solvent purification device (MBRAUN). The reactions were carried out under argon/nitrogen by using the Schlenck techniques. Thin layer chromatography (TLC) analysis was performed on pre-coated silica gel aluminium-backed plates (silica gel $60F_{254}$). The organic compounds were purified using flash column chromatography on silica gel (230-400 mesh). ^{l}H and ^{13}C-NMR spectra were recorded on Bruker-300, Bruker-400 and Bruker-500 spectrometers, and the spectra were referenced internally using residual proton solvent resonances relative to tetramethylsilane (δ = 0 ppm). Infrared (IR) spectra were recorded in the range of 4000-200 cm^{-1} on a FT-IR BRUKER ATR VERTEX70 Spectrometer. Elemental analyses were performed at the "Service de microanalyse", CNRS, 91198 Gif-sur-Yvette, France.

N.B.: As the organic ligands contain nitrile functional groups, all the experiments have been performed with great precautions, particularly considering the release of the HCN gas and related derivatives, which are poisonous and possibly toxic at low levels. Therefore, all the experiments related mainly to the synthesis should be handled in suitable protective methods. In this regard, all the waste involving nitrile compounds were destroyed using a specific basic bath containing a saturated ethanol solution of KOH with an aqueous NaOCl solution, and the glassware was cleaned using the bath with the basic ethanol and water (1:1 v/v) solution of KOH.

1.2 - Synthesis of Ligands

A - Synthesis of Triazole Ligand napht-trz.

The N-(1,2,4-triazol-4-yl)-1,8-naphthalimide (napht-trz) ligand was prepared according to a modified synthetic strategy (Scheme S1).[1] 4H-1,2,4-triazol-4-amine (5g, 0,059 mol) was added to a solution of 1,8-naphthalic anhydride (4 g, 0,02 mol) in acetic acid (40 mL). The reaction mixture was refluxed for 24 hours, and then the solution was allowed to cool and remain at room temperature for overnight. The resulting pale yellow crystalline compound

was filtered, and further washed with water (3 x 50 mL) and ether (3 x 25 mL), and finally dried under vacuum.Yield: 4.43 g, 84.09%.

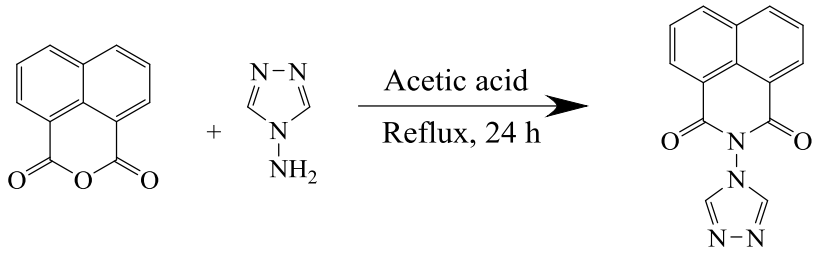

Scheme S1. Synthesis of the triazole ligand napht-trz

^{1}H NMR (DMSO, 298 K, 300 MHz): δ (ppm) 8.79 (s, 2H, trz-H), 8.61(d, 4H, 2X napht-H), 7.95 (t, 2H, napht-H) (Figure S1).

^{13}C NMR (DMSO, 298 K, 500 MHz): δ (ppm) 161.3, 143.3, 135.8, 131.8, 131.6, 127.5, 127.4, 121.5 (Figure S2 & S3).

IR (ν, cm^{-1}): 3134.84, 3057.77, 1718.02, 1681.50, 1659.25, 1582.25, 1515.38, 1438.25, 1391.54, 1326.11, 1234.98, 1222.29, 1174.97, 1152.29, 1137.32, 1118.58, 1077.69, 1065.58, 1031.08, 951.38, 890.96, 853.34, 803.73, 726.49, 696.52, 619.24, 533.03, 465.69, 425.18 (Figure S10).

B - Cyanocarbanion Ligand.

The potassium 1,1,3,3-tetracyano-2-thiomethylpropenide (K(tcnsme)) was synthesized in two steps according to the modified literature method (Scheme S2).[2] In the first step, 2-[(bis-methylthio)methylene]malononitrile was synthesized from malononitrile and alkyl halide following the modified reported methods. Then, the potassium [1,1,3,3-tetracyano-2-thiomethylpropenide] salt [K(tcnsme)] was obtained from the reaction between the corresponding ketene thioacetal with malononitrile in the presence of potassium tert-butoxide.

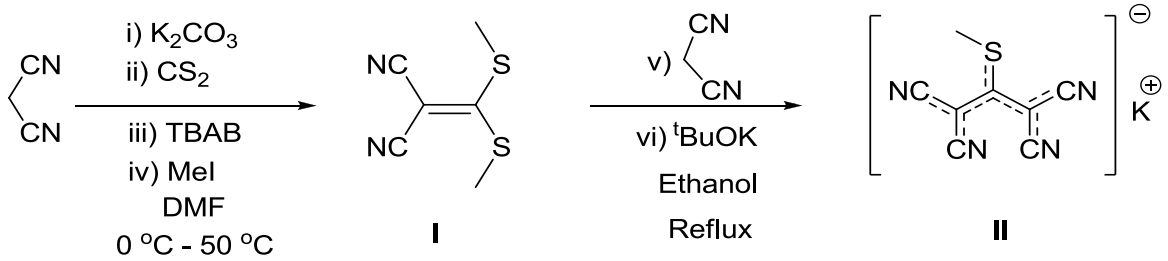

Scheme S2. Synthesis of K(tcnsme).

First Step. Synthesis of 2-[(bis-methylthio)methylene]malononitrile (I). A suspension of K_2CO_3 (8.37 g, 60.55 mmol) in DMF (25 mL) was treated with the addition of malononitrile (4.0 g, 60.55 mmol). The mixture was cooled down to 0 ^oC, and CS_2 (3.6 mL, 66.6 mmol) was added dropwise. The resulting yellow suspension was stirred at 20 ^oC for 10 minutes, after which methyl iodide (121.1 mmol, 7.6 mL) and tetrabutylammonium bromide (4 g, 10 mmol) were added over 30 minutes. The reaction mixture was stirred for 2 hours at 50 ^oC, and subsequently for an additional 24 to 48 hours at room temperature while monitoring the reaction status with TLC (2:98 ethyl acetate: hexane). The final mixture was diluted with water (200 mL) and extracted with dichloromethane (4×200 mL); the combined organic layers were washed with Brine solution (100 mL) and dried over $MgSO_4$, then filtered and concentrated under reduced pressure. The crude product was purified by chromatography on silica gel [hexane/EtOAc, 10:0 to 9.5:0.5 (v/v)] to provide 2-[(bis-methylthio)methylene]malononitrile. Yield: 7.725 g, 75 %**.** ^1H NMR (300 MHz, $CDCl_3$): *δ*, 2.76 (s, 6H, -SCH_3) (Figure S4). ^{13}C NMR (300 MHz, $CDCl_3$): *δ*, 184.0 (-$\underline{C}(S\text{-}Me)_2$), 112.8 (-$\underline{C}N$), 76.3 (-$\underline{C}(CN)_2$) 19.3 (-$SCH_3$) (Figure S5). IR data (ν, cm^{-1}) : 3003w, 2926w, 2827w, 2417w, 2351w, 2308w, 2209s, 1489w, 1442s, 1417s, 1316m, 1211w, 983w, 960w, 922m, 869s, 708w, 610w, 475w, 457w (Figure S8).

Second step. Synthesis of potassium [1,1,3,3-tetracyano-2-thiomethylpropenide] salt (K(tcnsme)). An ethanol solution (10 mL) of malononitrile (0.66 g, 10 mmol) and tBuOK (1.12 g, 10 mmol) was added dropwise to the solution of the 2-[bis(methylthio)methylene]malononitrile (10 mmol, 1.7 g) in ethanol (30 mL) at 30^0C. The resulting solution was refluxed for 1h, and then the reaction mixture was cooled down to room temperature, and finally kept at 4^0C for two days. The resulting compound was filtered on a sintered-glass funnel and washed with distilled diethyl ether, and ultimately dried under vacuum to obtain the yellow crystalline powder of K(tcnsme) salt in good yield. Yield: 1.516 g, 67 %. ^1H NMR (300 MHz, Acetone-D_6): *δ*, 2.54 (s, 3H -CH_3) (Figure S6). ^{13}C NMR (500 MHz, Acetone-D_6): *δ*, 170.2 (-$\underline{C}(S\text{-}Me)_2$), 119.0 (-CN), 117.0 (-CN), 53.6 (-$\underline{C}(CN)_2$), 18.4 (-SCH_3) (Figure S7). IR data (ν, cm^{-1}): 2188s, 1450s, 1426m, 1329w, 1248w, 955w, 928w, 857w, 642w, 576w, 529w, 470w (Figure S9).

1.3 - Synthesis of the [Fe(napht-trz)$_6$](tcnsme)$_2$.4CH$_3$CN (C1) complex. An acetonitrile solution (15 mL) of $Fe(BF_4)_2.6H_2O$ (40.5 mg, 0.12 mmol) and napht-trz (192 mg, 0.72 mmol) was refluxed for 4 hours. The K(tcnsme) salt (55 mg, 0.24 mmol) was added to the above reaction mixture, and then the resulting solution was further refluxed for 2 hours, and finally

the solution was cooled to room temperature and kept at 4°C for 20 days to obtain yellow crystals. Yield: 137 mg, 41.14 %. Anal. Calcd for $C_{108}H_{66}FeN_{36}O_{12}S_2$: C, 59.5; H, 3.1; N, 23.1 %. Found: C, 59.1; H, 3.0; N, 23.5 %. IR (ν, cm^{-1}): 3148, 2190, 1718, 1693, 1587, 1515, 1399, 1328, 1232, 1175, 1135, 1077, 1064, 1030, 987, 943, 895, 869, 840, 804, 726, 699, 627, 532 (Figure S11).

1.4 - [Cu(napht-trz)$_6$](tcnsme)$_2$.4CH$_3$CN (C2). Complex C2 has been prepared using similar procedure than compound C1: an acetonitrile solution (15 mL) of $Cu(BF_4)_2.6H_2O$ (28.5 mg, 0.12 mmol) and napht-trz (192 mg, 0.72 mmol) was refluxed for 2 hours. The K(tcnsme) salt (55 mg, 0.24 mmol) was added to the above reaction mixture, and then the resulting solution was further refluxed for 2 hours, and finally the solution was cooled to room temperature and kept at 4°C for 20 days to obtain green crystals. Yield: 221 mg, 83 %. Anal. Calcd for $C_{108}H_{66}cCuN_{36}O_{12}S_2$: C, 59.3; H, 3.0; N, 23.1 %. Found: C, 58.9; H, 3.0; N, 23.5 %. IR (ν, cm^{-1}): 3162, 3142, 2189, 1727, 1693, 1668, 1587, 1516, 1451, 1400, 1371, 1329, 1232, 1174, 1135, 1077, 1062, 1030, 1001, 973, 948, 895, 860, 840, 804, 727, 699, 642, 627, 573, 532, 476, 458, 436, 418 (Figure S12).

2 - NMR Spectra

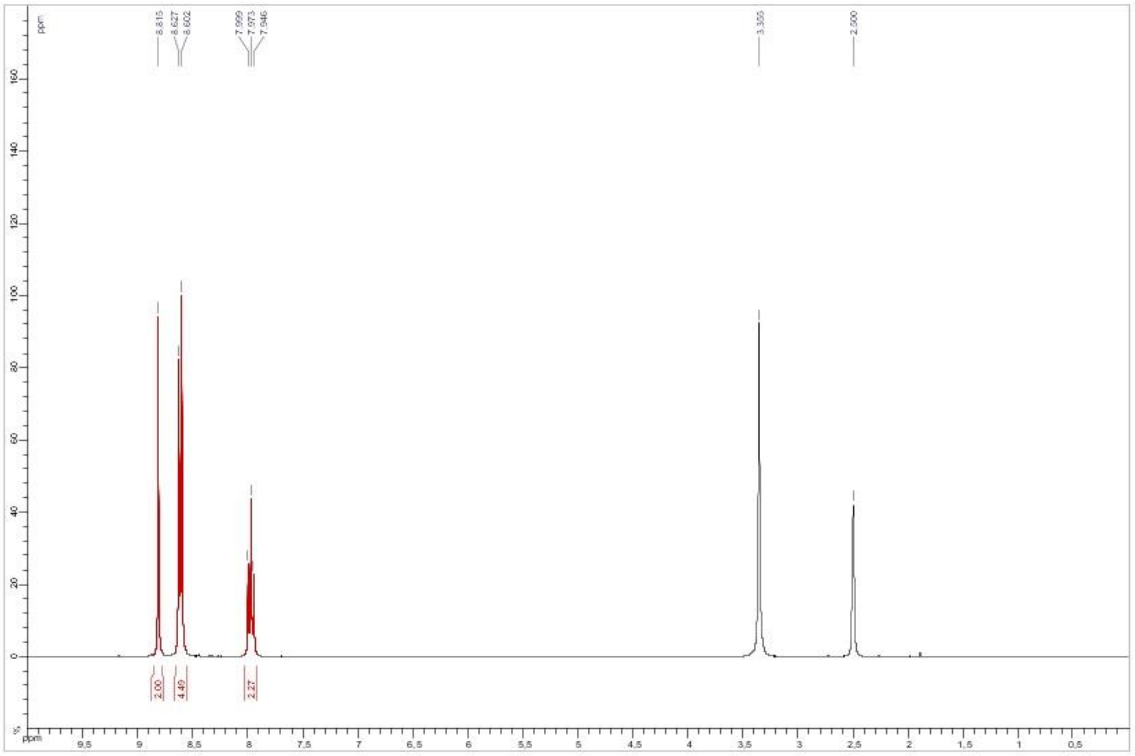

Figure S1. ^{1}H NMR (DMSO-D$_6$, 300 MHz) spectrum of napht-trz.

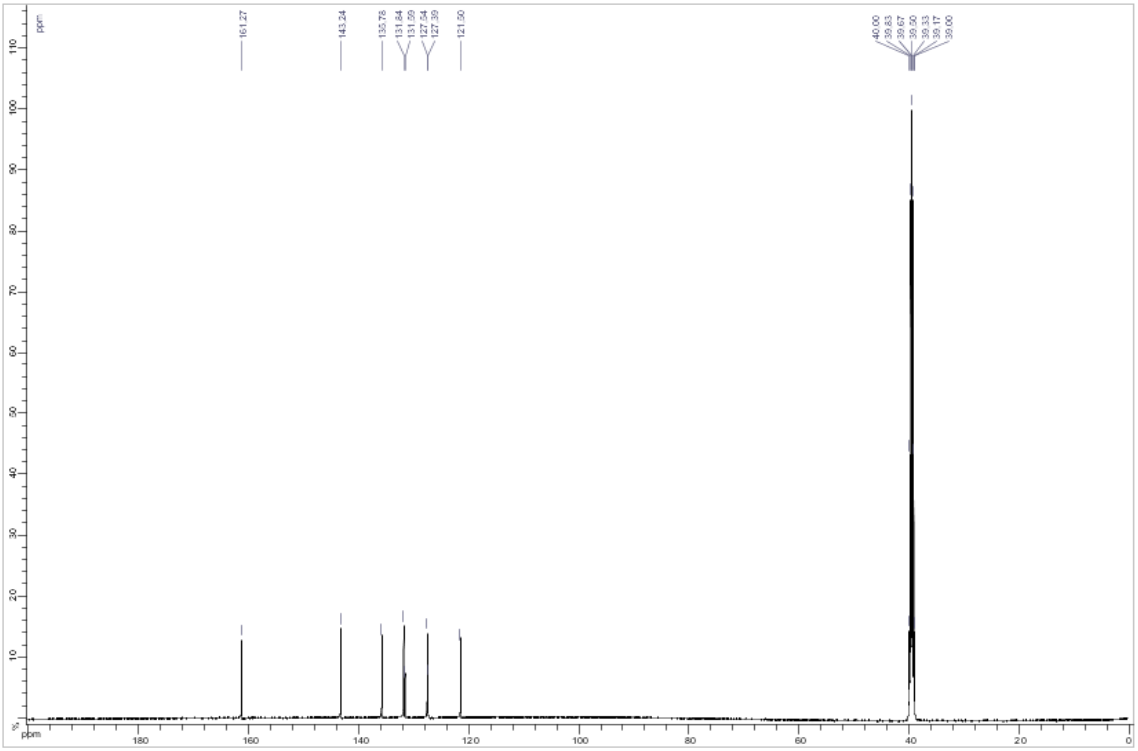

Figure S2. ^{13}C NMR (DMSO-D_6, 500 MHz) spectrum of napht-trz.

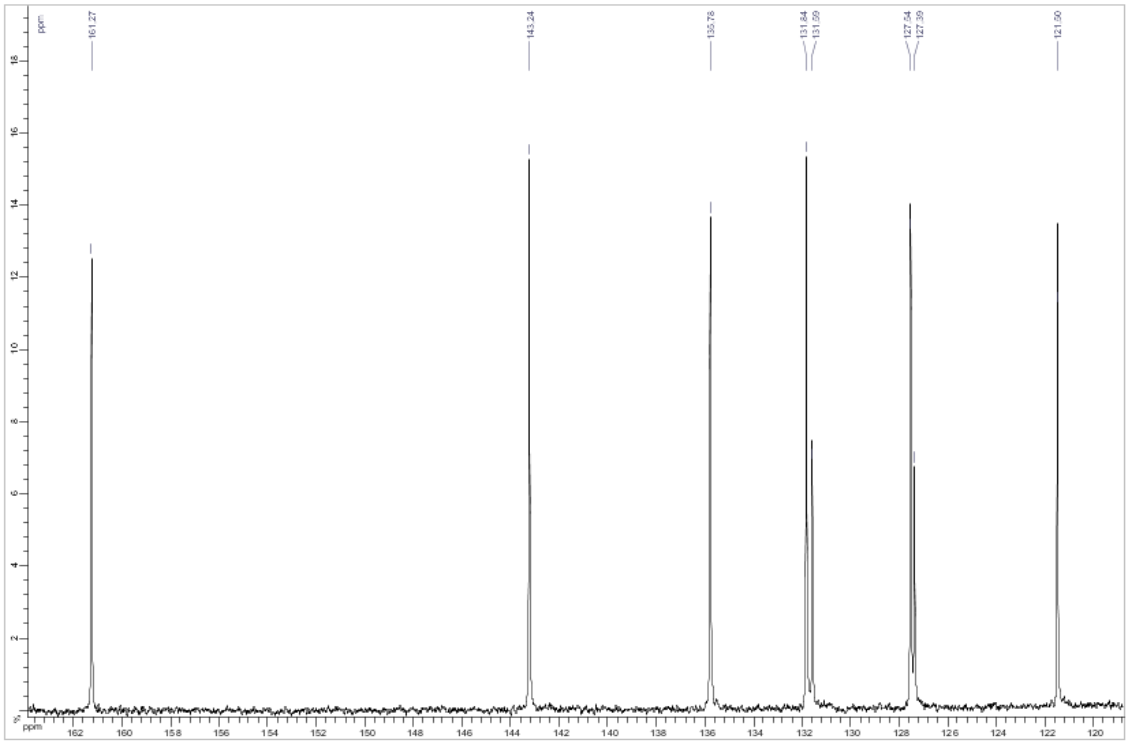

Figure S3. ^{13}C NMR (DMSO-D_6, 500 MHz) spectrum of napht-trz - aromatic region.

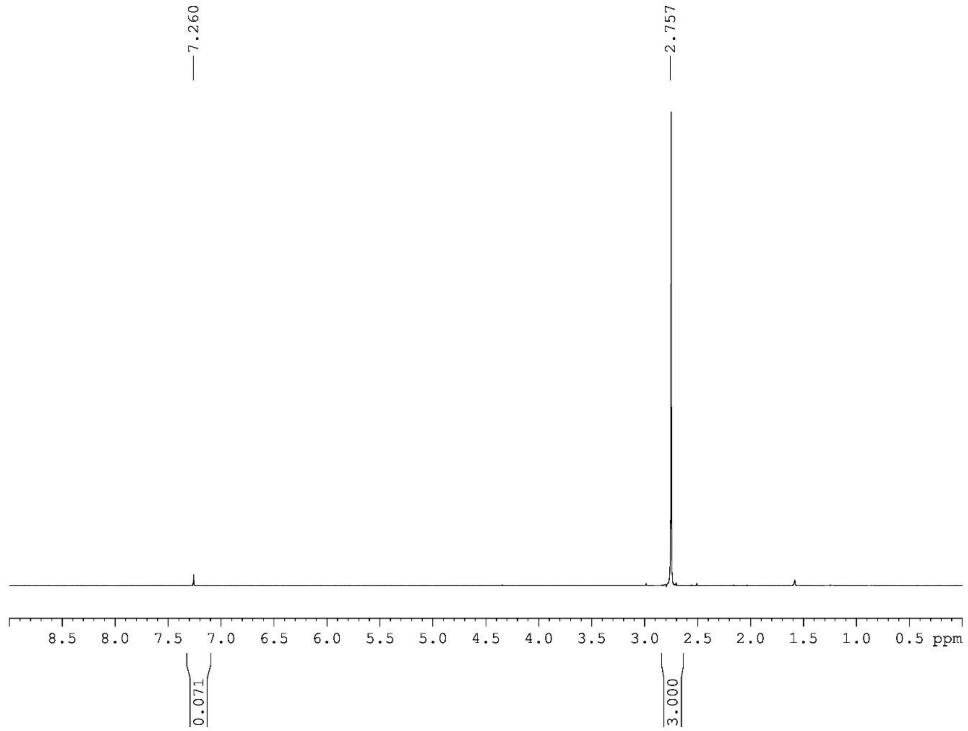

Figure S4. ^{1}H NMR (300 MHz, $CDCl_3$) of 2-[bis(methylthio)methylene]malononitrile (I).

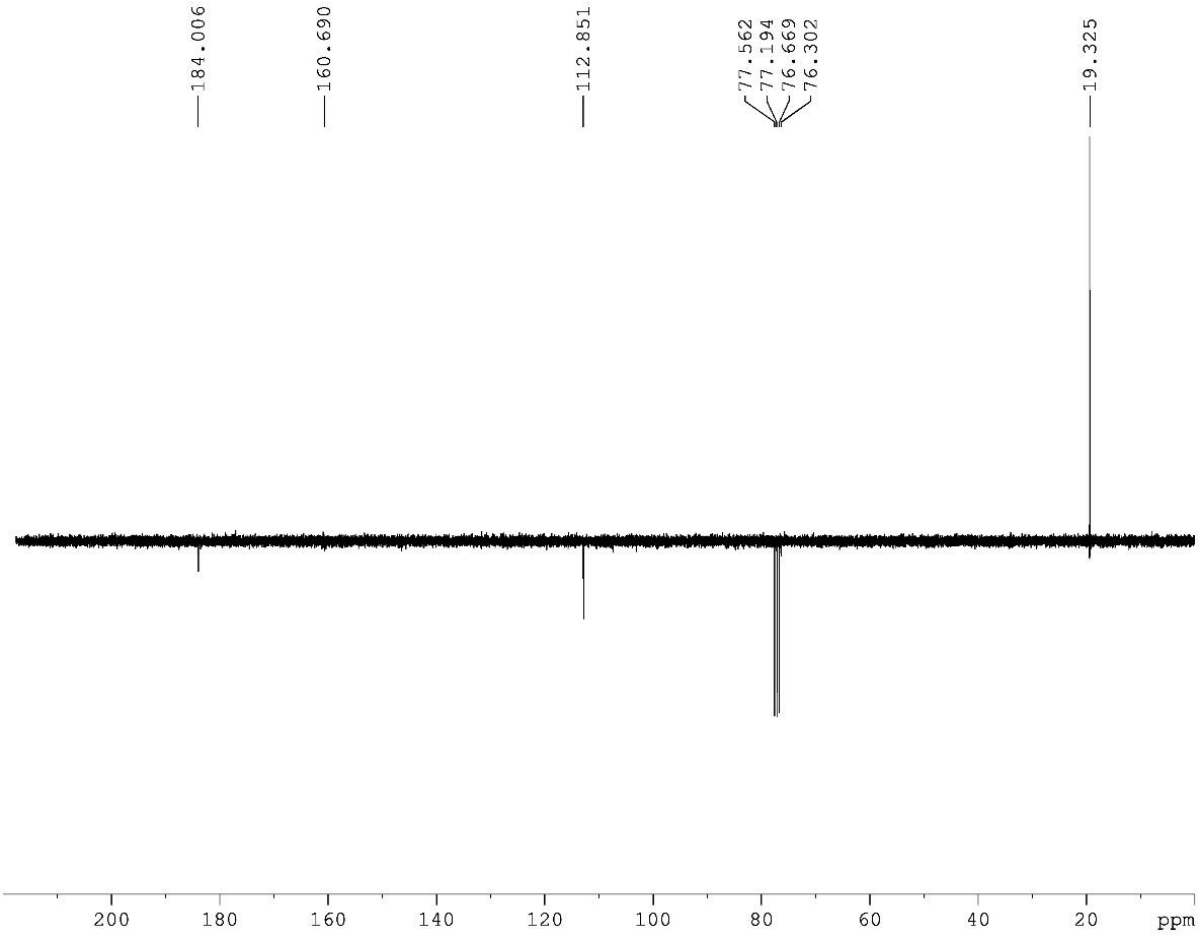

Figure S5. ^{13}C NMR (300 MHz, $CDCl_3$) of 2-[bis(methylthio)methylene]malononitrile (I).

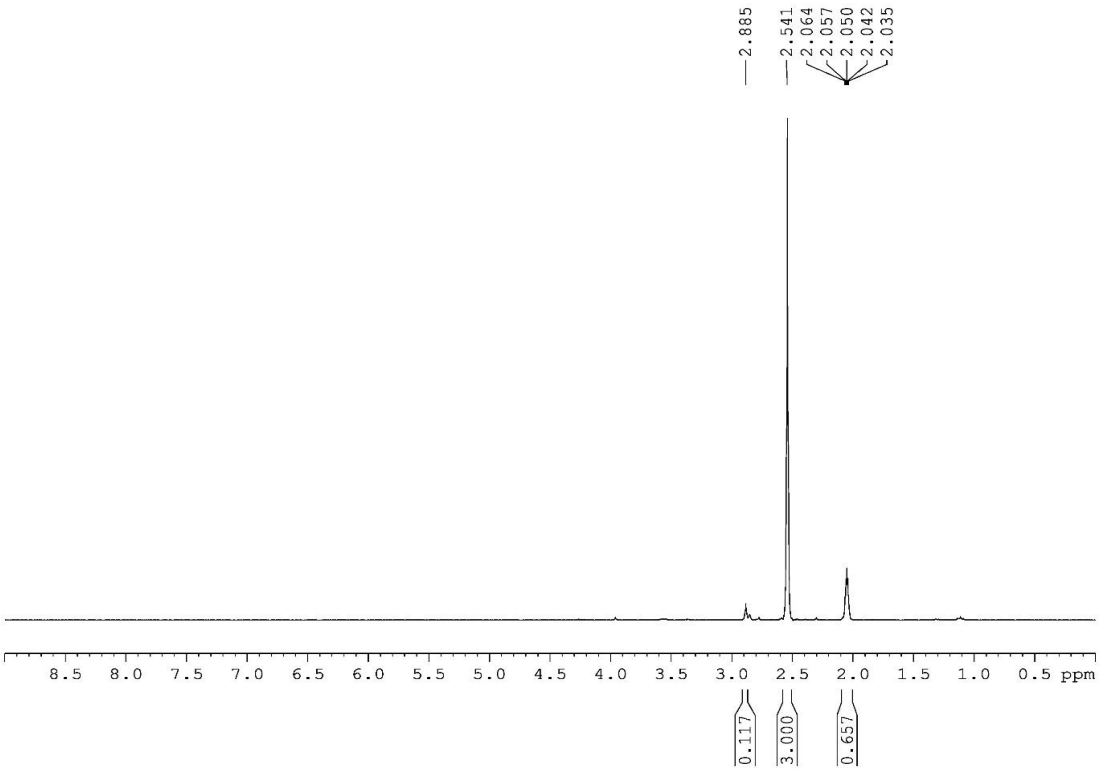

Figure S6. ^{1}H (300 MHz, Acetone-D_6) of K(tcnsme) salt (II).

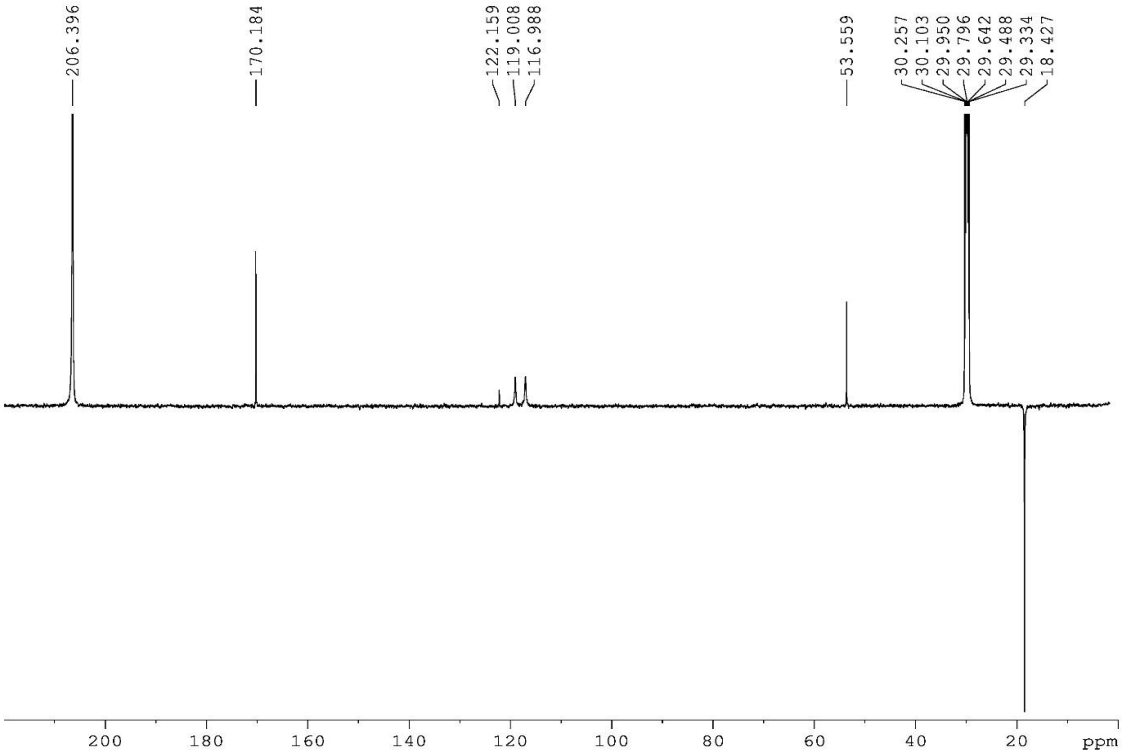

Figure S7. ^{13}C NMR (500 MHz, Acetone-D_6) of K(tcnsme) salt (II).

3 - Infrared Spectra

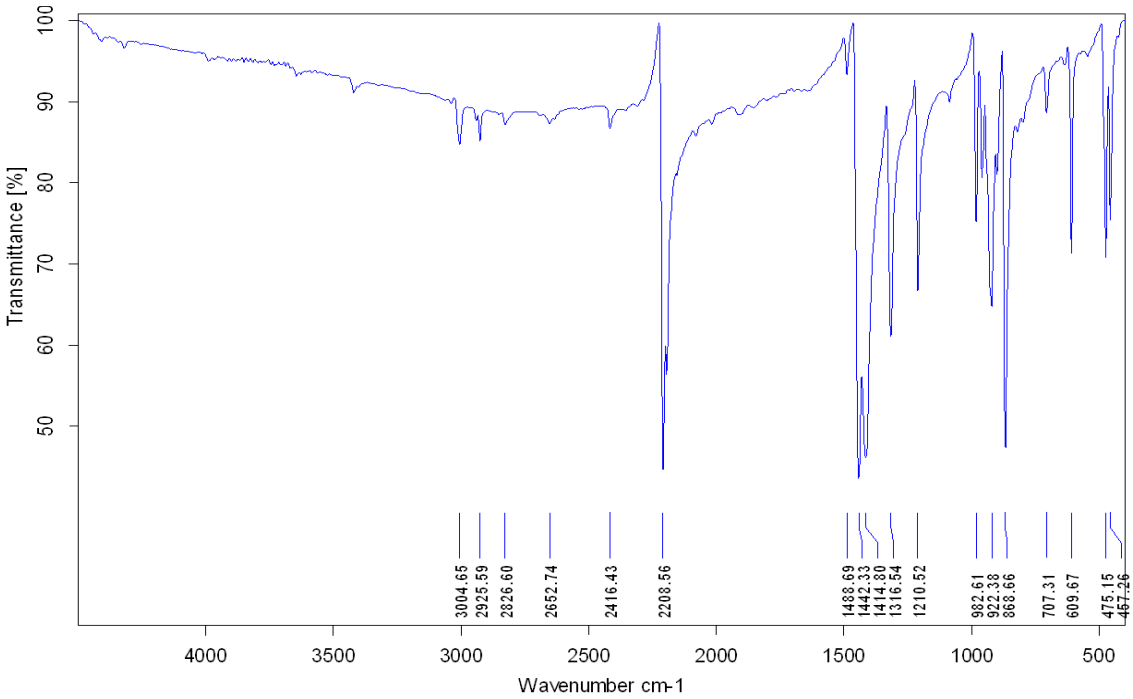

Figure S8. IR Spectrum of 2-[bis(methylthio)methylene]malononitrile (I).

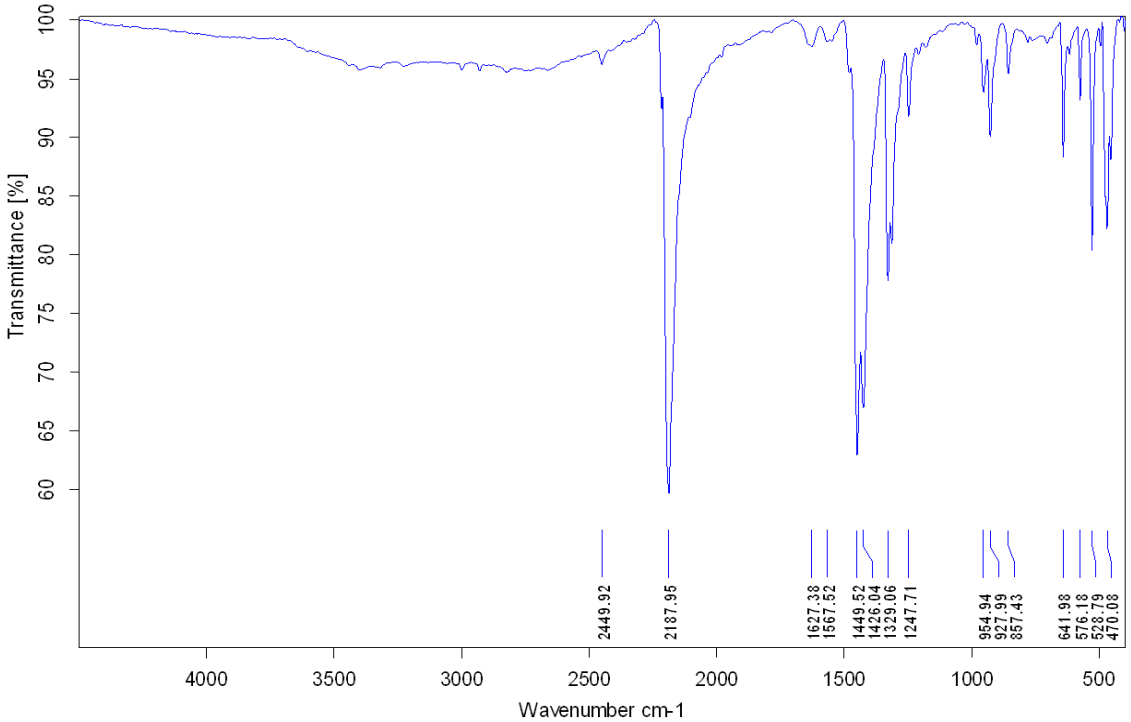

Figure S9. IR Spectrum of K(tcnsme) salt (II).

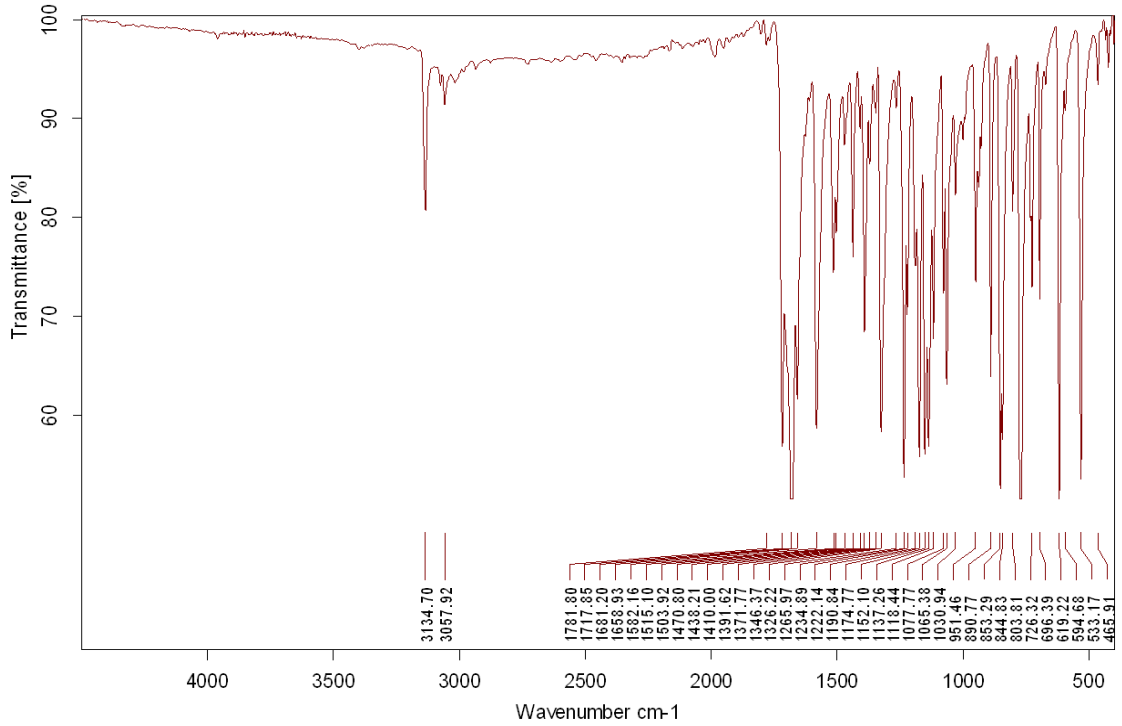

Figure S10. IR spectrum of napht-trz.

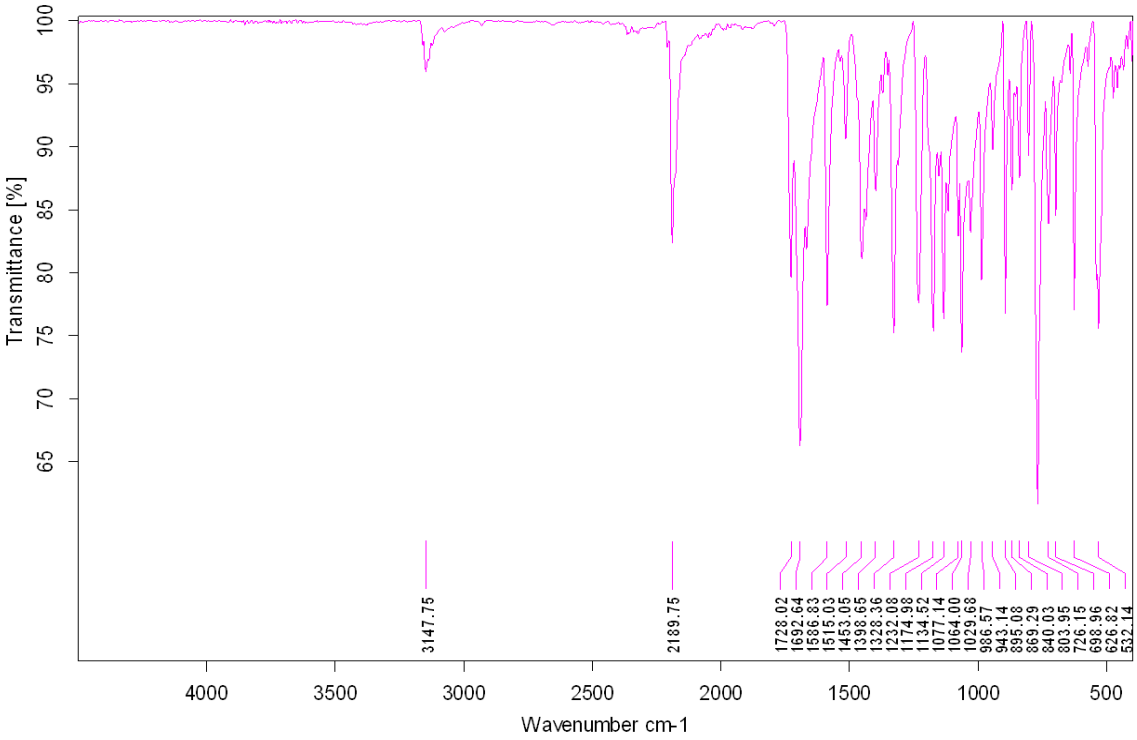

Figure S11. IR spectrum of complex $[Fe(napht\text{-}trz)_6](tcnsme)_2.4CH_3CN$ (**C1**).

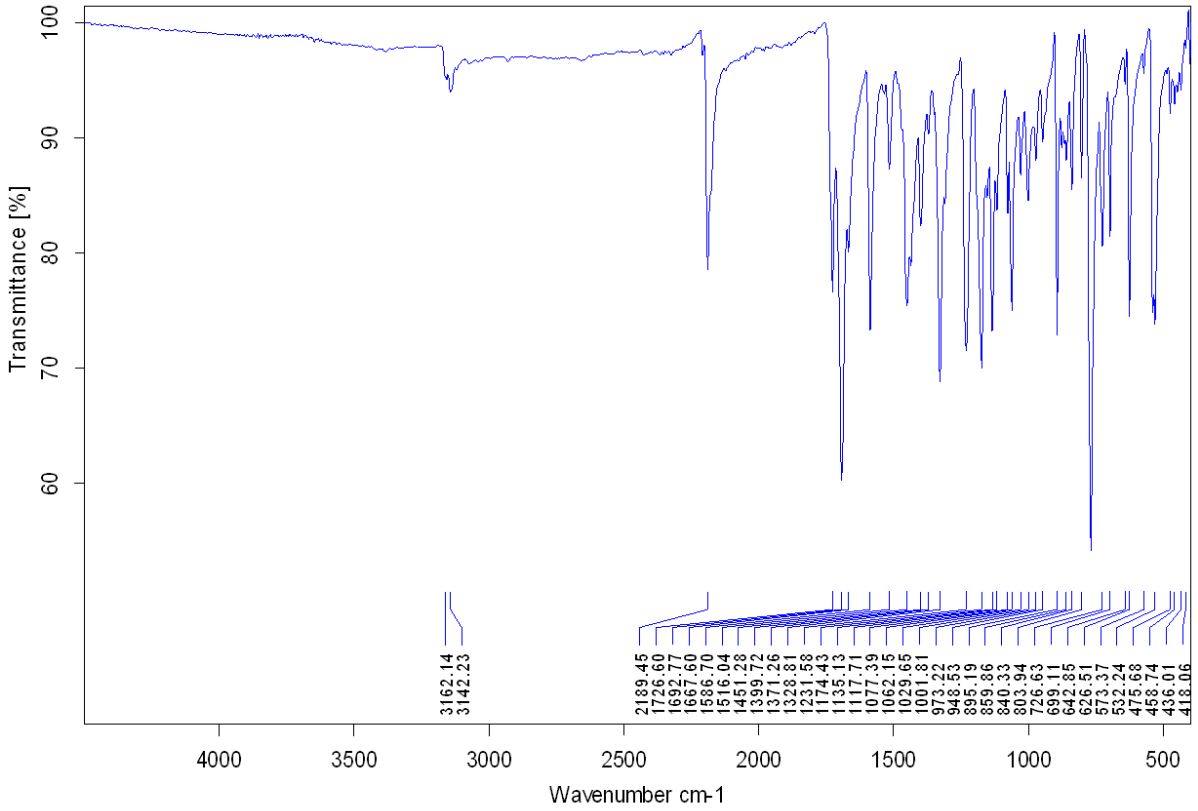

Figure S12. IR spectrum of complex $[Cu(napht\text{-}trz)_6](tcnsme)_2.4CH_3CN$ (**C2**).

4 - Physical Measurements and Characterizations

4.1 - X-ray Crystallography. Single crystal X-ray diffraction studies were performed at 100 K and 293 K on Xcalibur 2 κ-CCD diffractometer using Mo Kα radiation (λ = 0.71073 Å). The corresponding structures were solved by direct methods with the SHELXS program and refined on F^2 by weighted full matrix least-squares methods using the SHELXL program.[3] All non-hydrogen atoms were refined anisotropically, hydrogen atoms were located in difference Fourier maps, and treated using a riding model. Crystallographic data and refinement details are provided in Table S1.

Table S1. Crystal data and structural refinement parameters for compound **C1.**

Compound	**C1**	
Temperature / K	296(2)	100(2)
Color	Yellow	Red
Empirical formula	$C_{108}H_{66}FeN_{36}O_{12}S_2$	$C_{108}H_{66}FeN_{36}O_{12}S_2$
Formula weight /g.mol^{-1}	2179.94	2179.94
Wavelength / Å	0.71073 Å	0.71073 Å
Crystal system	Monoclinic	Monoclinic
Space group	*P2$_1$/c*	*P2$_1$/c*
a / Å	9.0646(7)	8.9139(4)
b / Å	16.0413(11)	15.9285(9)
c / Å	35.656(2)	35.1158(18)
β (°)	90.122(7)	90.474(5)
Volume / Å^3	5184.6(6)	4985.7(4)
Z	2	2
D_{calc} / g.cm^{-3}	1.396	1.452
Abs. coef. / cm^{-1}	2.67	2.78
F(000)	2240	2240
Crystal size / mm^3	0.28 × 0.12 × 0.09	0.28 × 0.12 × 0.09
2θ range / °	6.83 to 58.65	6.86 to 58.43
Refl. collected	24763	21868
Unique refl. / Rint	11340 / 0.0942	11291 / 0.0838
Data / restr. / N_v	5194 / 0 / 721	6248 / 0 / 721
Final R indexes [I>2σ (I)]	R = 0.1074, wR = 0.2252	R = 0.0948, wR = 0.1838
[c]GooF	1.105	1.092
$\Delta\rho_{max/\,min}$ / eÅ^{-3}	0.407 / - 0.548	0.688 / -1.345
CCDC No.	1565194	1565195

[a]$R = \sum |F_o - F_c| / F_o$. [b]$wR = \{\sum[w(F_o^2 - F_c^2)^2] / \sum[w(F_o^2)^2]\}^{1/2}$. [c]$GooF = \{\sum[w(F_o^2 - F_c^2)^2] / (N_{obs} - N_{var})\}^{1/2}$

Table S2. Fe-N bond lengths (Å) and N-Fe-N (°) bond angles at 293K and 100 K for complex **C1**.

Compound	**C1**	
T / K	**293**	**100**
Fe1-N1	2.200(4)	1.999(4)
Fe1-N2	2.190(4)	1.993(4)
Fe1-N3	2.176(4)	1.994(4)
<Fe-N>	**2.189(4)**	**1.995(4)**
N1-Fe1-N1$^{(a)}$	180.0	180.0
N2-Fe1-N2$^{(a)}$	180.0	180.0
N3-Fe1-N3$^{(a)}$	180.0	180.0
N1-Fe1-N3	87.51(16)	88.11(17)
N1$^{(a)}$-Fe1-N3$^{(a)}$	87.51(16)	88.11(17)
N1-Fe1-N3$^{(a)}$	92.49(16)	91.89(17)
N1$^{(a)}$-Fe1-N3	92.49(16)	91.89(17)
N1-Fe1-N2	88.20(16)	88.85(16)
N1$^{(a)}$-Fe1-N2$^{(a)}$	88.20(16)	88.85(16)
N1-Fe1-N2$^{(a)}$	91.81(16)	91.15(16)
N1$^{(a)}$-Fe1-N2	91.81(16)	91.15(16)
N3$^{(a)}$-Fe1-N2$^{(a)}$	90.02(16)	91.16(16)
N3-Fe1-N2	90.02(16)	91.16(16)
N3$^{(a)}$-Fe1-N2	89.98(16)	88.84(16)
N3-Fe1-N2$^{(a)}$	89.98(16)	88.84(16)
$^{(b)}\Sigma$	17.28	16.8

Symmetry transformations used to generate equivalent atoms: (a) -x,-y,-z

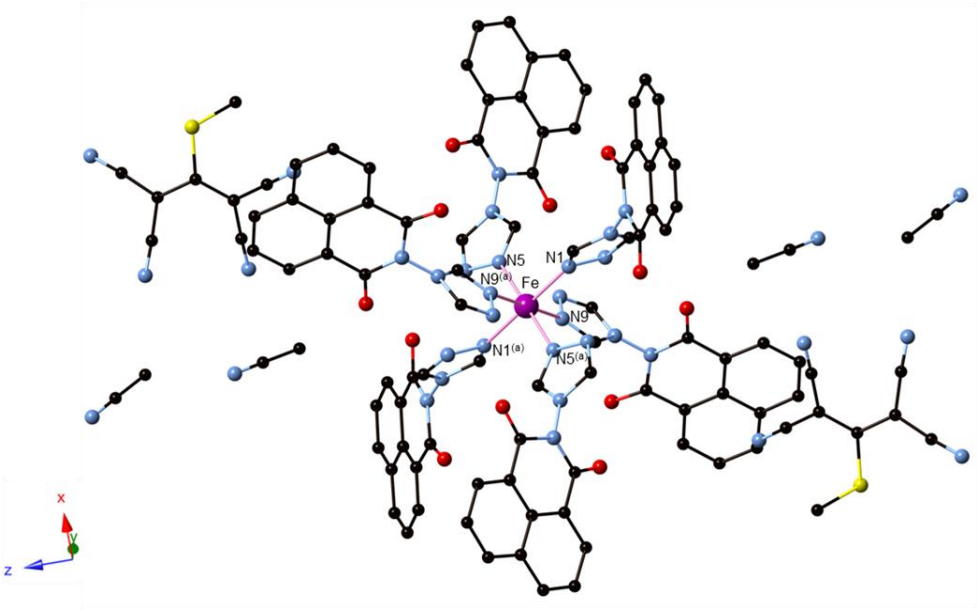

Figure S13. Molecular structure of the complex $[Fe(napht\text{-}trz)_6](tcnSMe)_2.4.CH_3CN$ (**C1**).

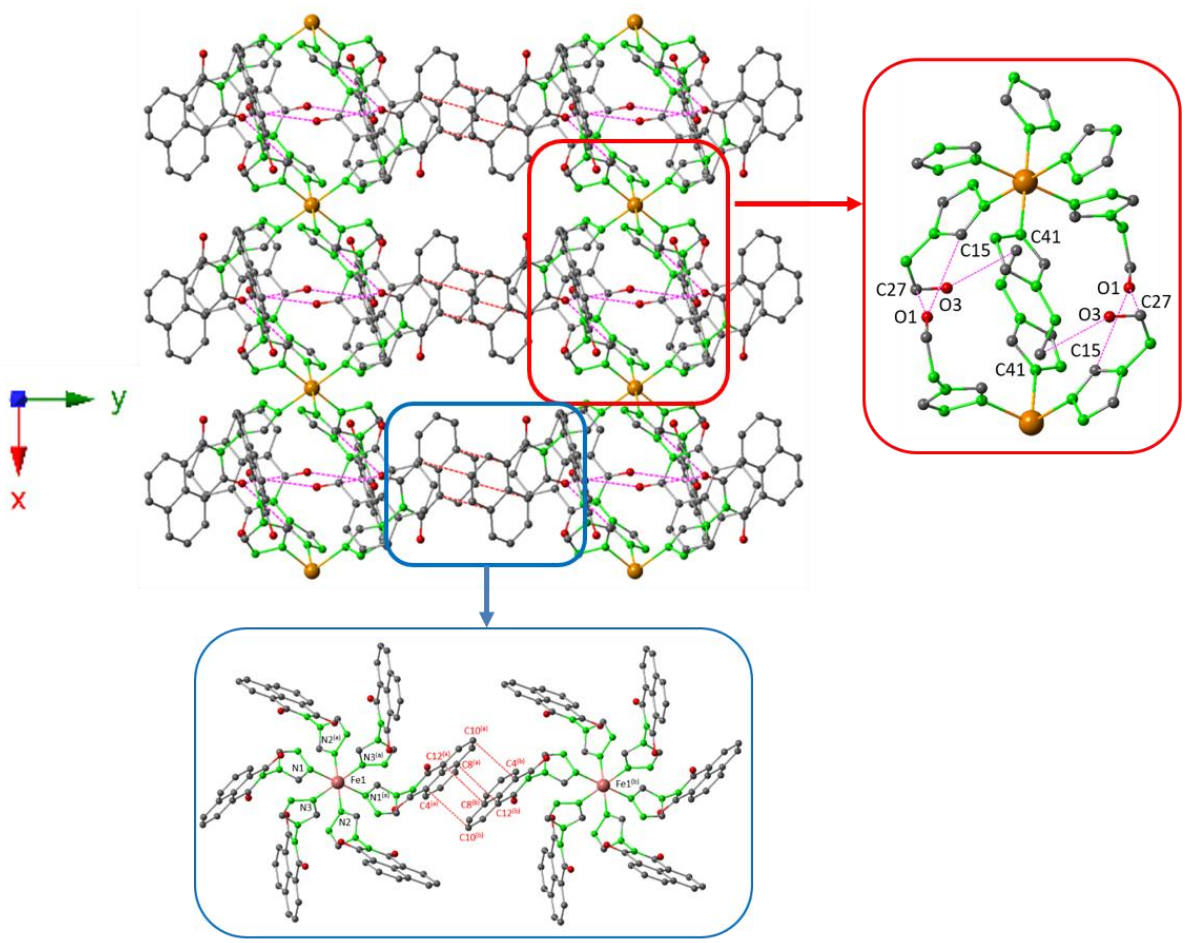

C4…C10: 3.538 Å (296 K) and 3.510 Å (100 K) ; C8…C12: 3.517 Å (296 K) and 3.506 Å (100 K); O…C: 3.20-3.30 Å. (a) = -x, -y, -z. (b) = x, 1+y, z

Figure S14. Intermolecular contacts in compound **C1** at 296 and 100 K.

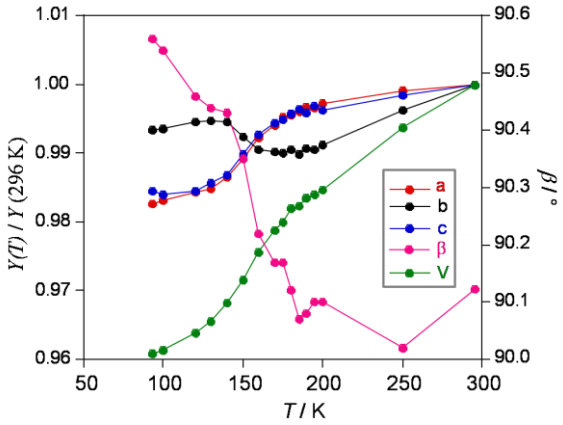

Figure S15. Thermal evolution of the lattice parameters of complex **C1**.

4.2 - Magnetic Properties. Magnetic susceptibility measurements were carried out in the temperature range 2-300 K with an applied magnetic field of 0.5 T on a polycrystalline sample of compound **C1** (with a mass of 4.25 mg) with a Quantum Design MPMS-XL-5 SQUID susceptometer. Consecutive cooling and warming scans at a scan rate of 0.4 K min^{-1} showed identical behaviours without any noticeable hysteresis. The photomagnetic study was performed by cooling the sample down to 10 K and then irradiating it with a green Diode Pumped Solid State Laser DPSS-532-20 from Chylas (λ = 532 nm, power = 20 mW) coupled *via* an optical fibre to the cavity of the SQUID magnetometer. When saturation of the magnetization was reached (after ca. 110 min, see supporting information), the laser was switched off and the sample was heated up to 300 K at a rate of 0.4 K min^{-1}. During the initial irradiation at 10 K, no significant decrease of the magnetic response due to heating of the sample was observed. The sample for the LIESST studies consisted of a thin layer of microcrystalline powder of the compound.

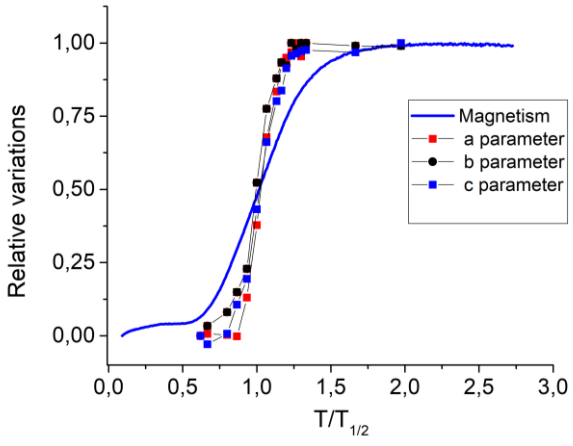

Figure S16. Relative thermal variation of the magnetic signal (blue line) and the lattice parameters *a*, *b* and *c* from which the HS fraction was extracted after subtraction of the normal thermal expansion. To compare them, the data were plotted all parameters as a function of the dimensionless parameter, $T/T_{1/2q}$, where $T_{1/2}$ is the transition temperature associated to each of them (150 K for structural parameters and 114 K for the magnetic response).

4.3 – Optical Studies. Optical absorption measurements were done on a 1:19 pellet mixture of **C1** and KBr and deduced from the transmission spectra obtained by using a Perkin Elmer (Lambda 950 nm) spectrometer. Sample temperature was controlled using a cold finger of a helium closed cycle cryostat. PL measurements performed in the temperature range 2-300 K have been done on **C1** as well as on **L1** and **C2** samples. All studies were obtained under the same protocol on single crystals by using the same light intensity 2 mW of excitation at wavelength λ_{ex} = 325 nm (3.815 eV) from a Spectra-Physics beamlock 2085 Argon laser. PL spectra were recorded by a monochromator Triax500 equipped with a CCD camera 1024 x 256 pixel.

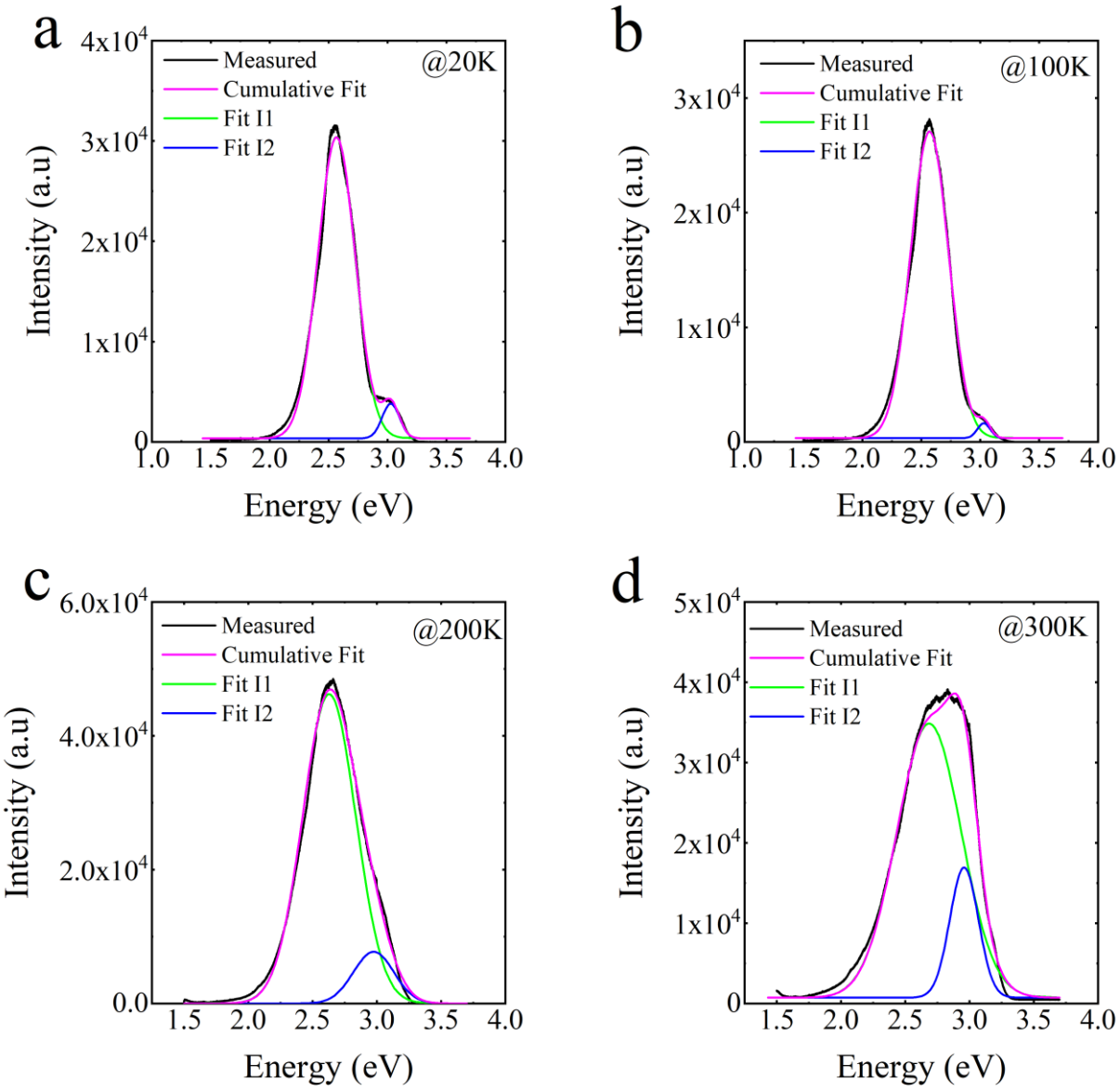

Figure S17. Examples of the fitting of temperature dependence fluorescence data of ligand **L1**, using two Gaussian functions.

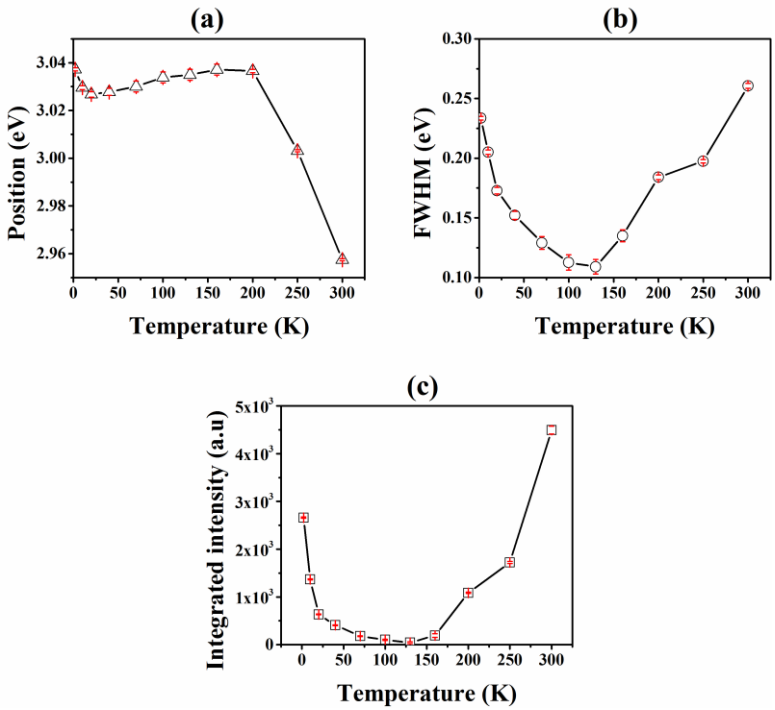

Figure S18. Thermal evolution of the (a) position, (b) FWHM and (c) integrated intensity of the fluorescence peak I2, of ligand **L1**.

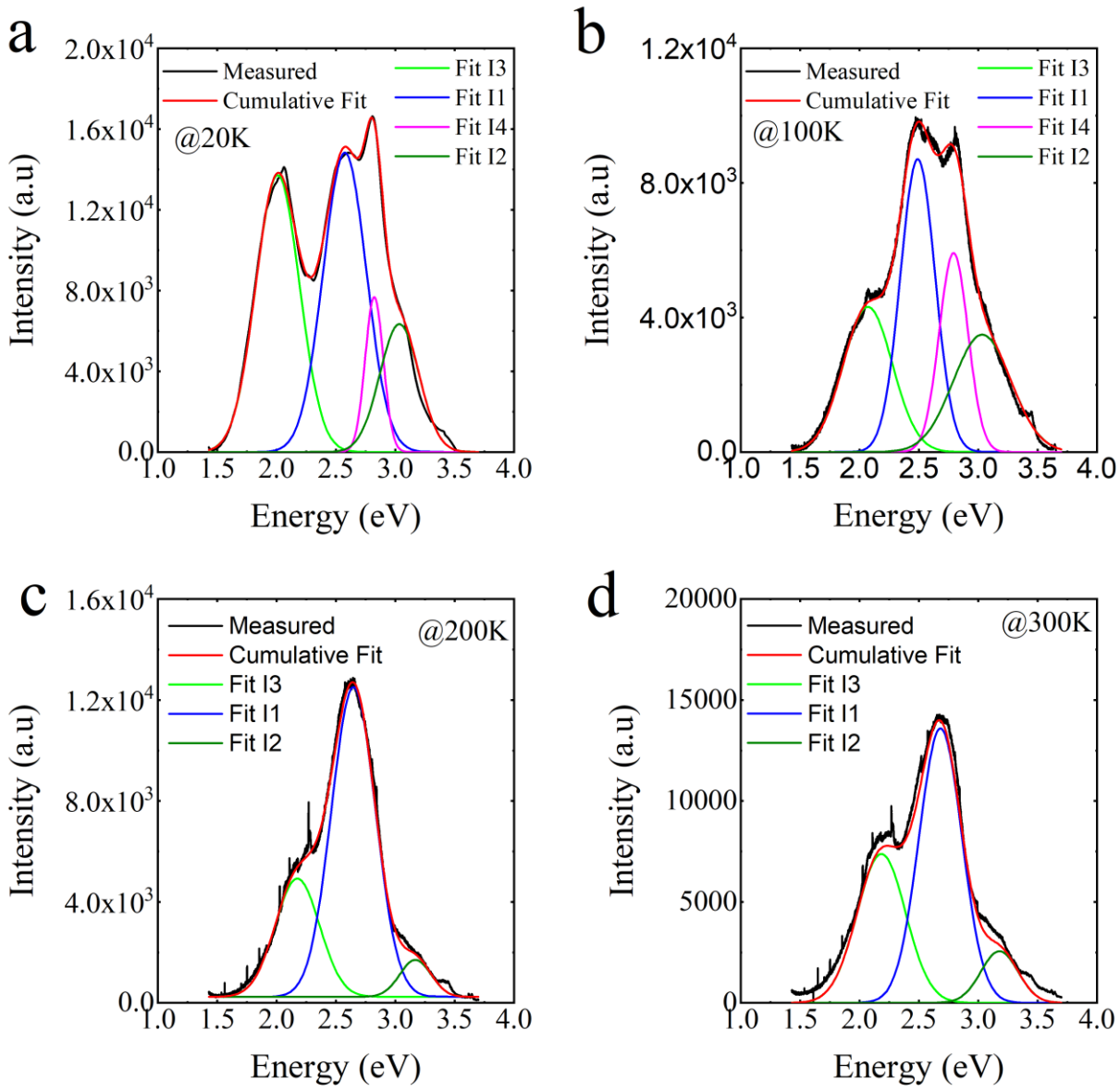

Figure S19. Examples of the fitting of temperature dependence of fluorescence data of complex **C1**, using multiple Gaussian functions.

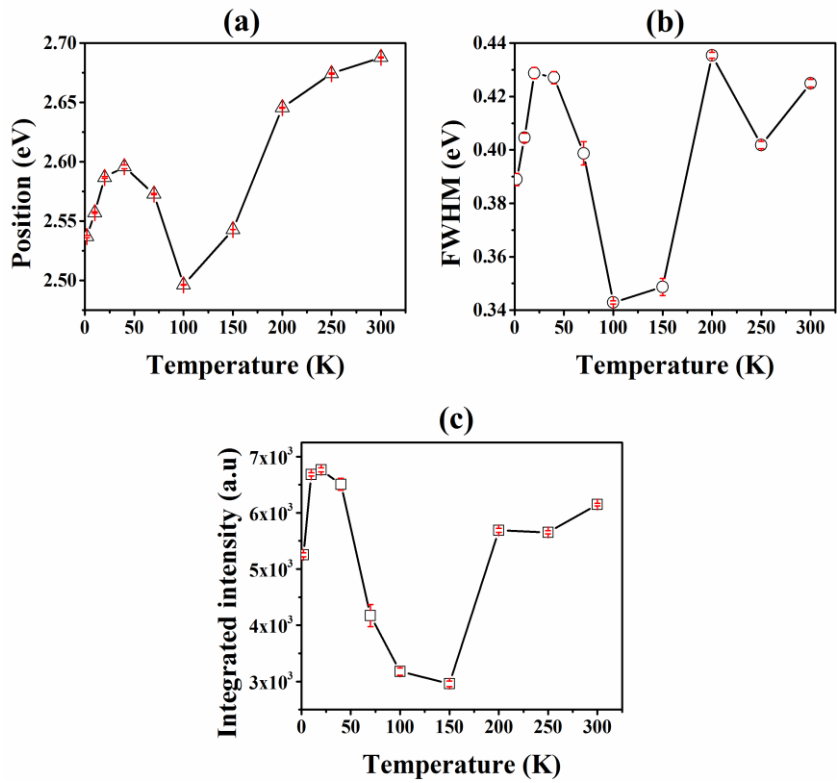

Figure S20. Thermal evolution of the (a) position, (b) FWHM and (c) integrated intensity of the emission peak I1, of **C1**.

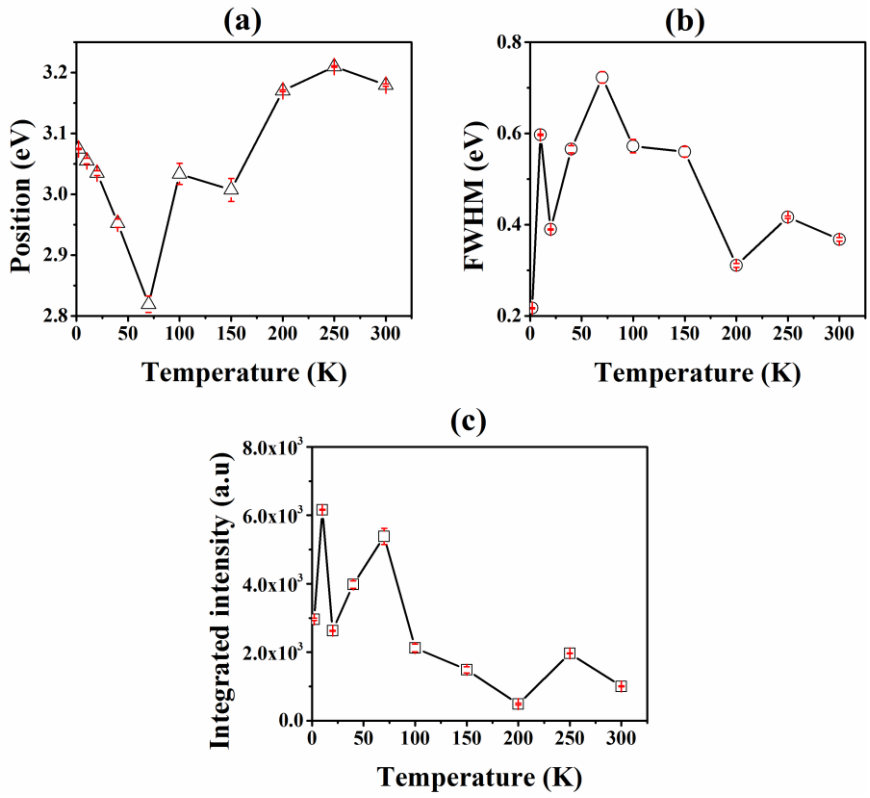

Figure S21. Thermal evolution of the (a) position, (b) FWHM and (c) integrated intensity of the emission peak I2, of **C1**.

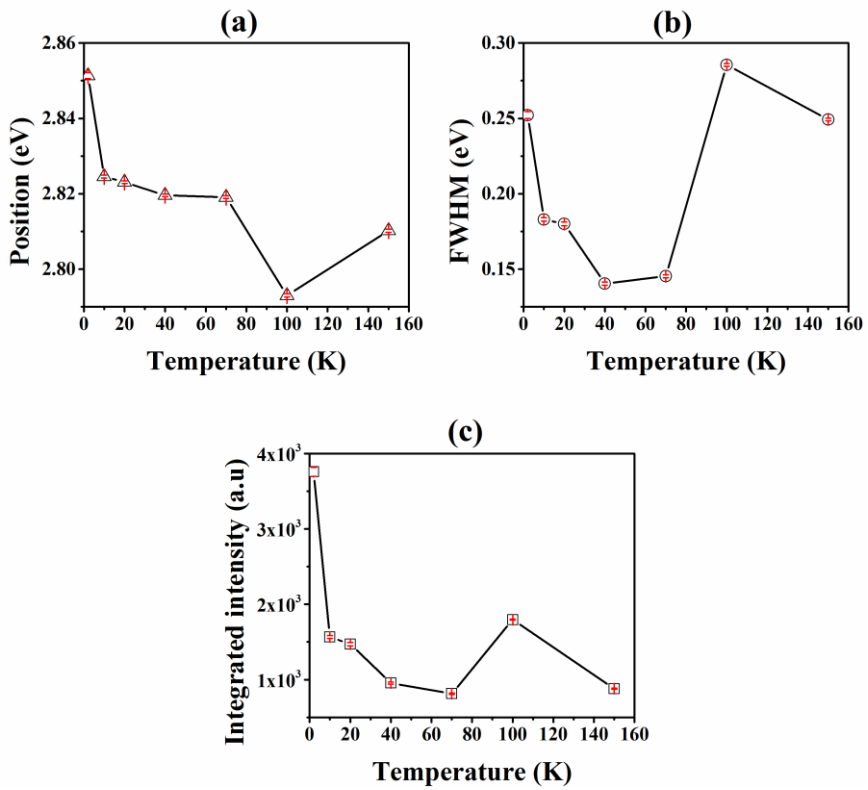

Figure S22. Thermal evolution of the (a) position, (b) FWHM and (c) integrated intensity of the emission peak I4, of **C1**.

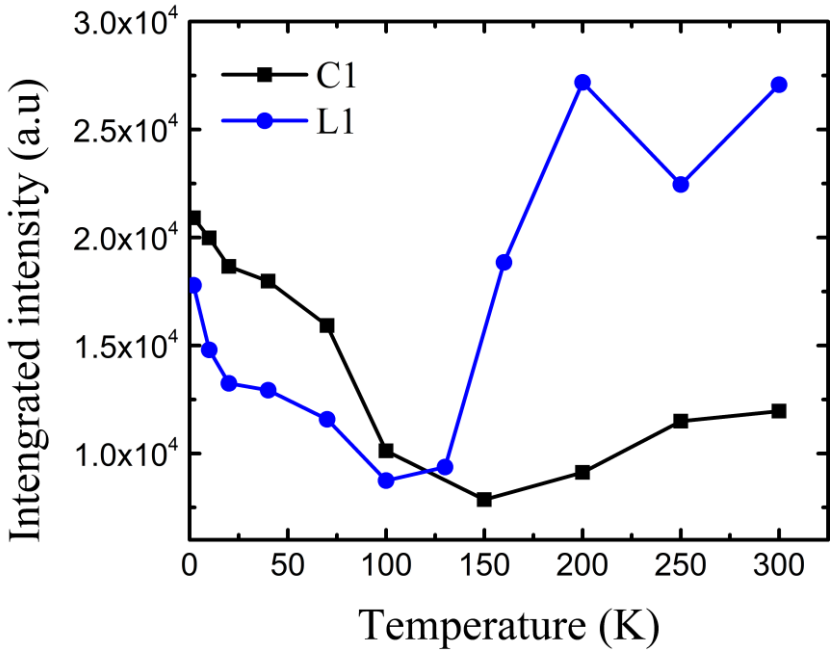

Figure S23. Temperature dependence of the overall integrated fluorescence intensity of **L1** (blue) and **C1** (black).

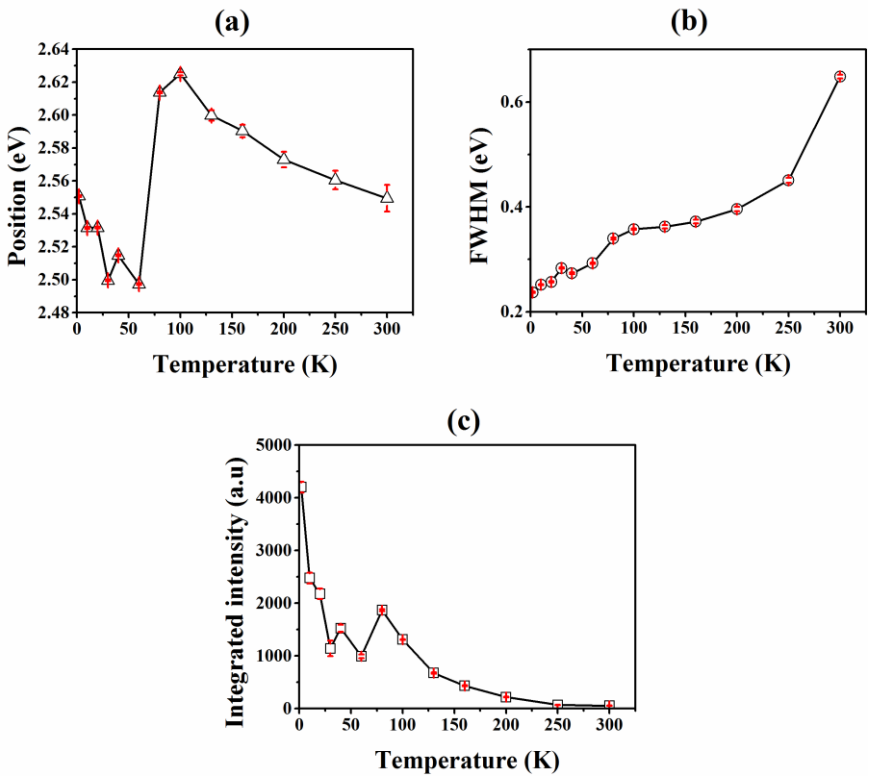

Figure S24. Thermal evolution of the (a) position, (b) FWHM and (c) integrated intensity of the fluorescence peak I1, of **C2**.

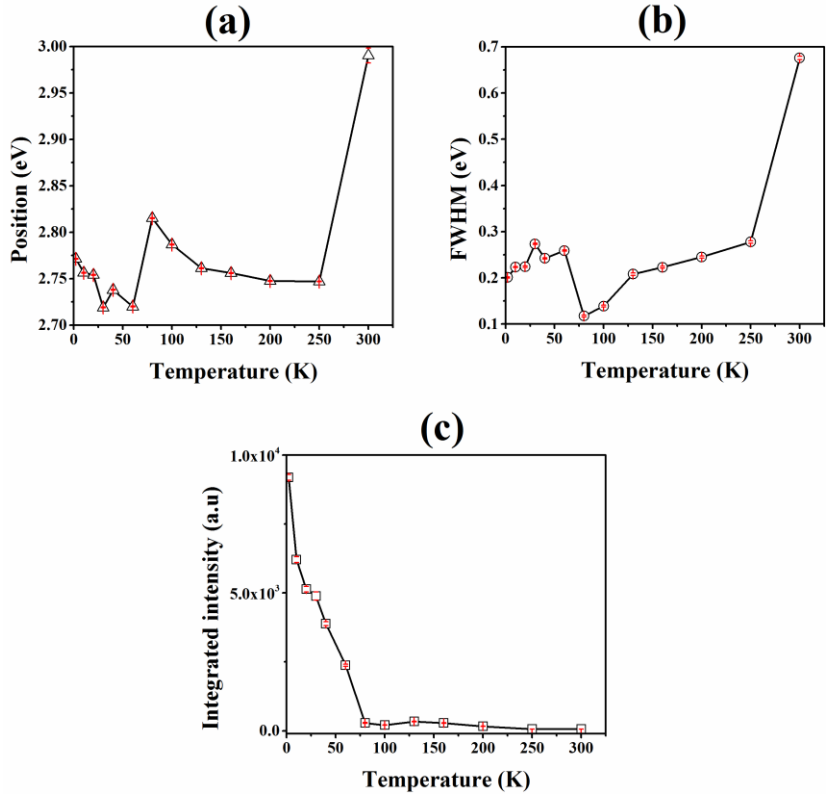

Figure S25. Thermal evolution of the (a) position, (b) FWHM and (c) integrated intensity of the fluorescence peak I2, of **C2**.

5 - References

1. (a) J. A. Kitchen, N. Zhang, A. B. Carter, A. J. Fitzpatrick, & G. G. Morgan, *J. Coord. Chem.*, **2016**. 69, 2024-2037; (b) S. Banerjee, J. A. Kitchen, S. A. Bright, J. E. O'Brien, D. C. Williams, J. M. Kelly, T. Gunnlaugsson. *Chem.Commun.*, **2013**, *49*, 8522; (c) S. Mallakpour, Z. Rafiee, *Journal of Applied Polymer Science*, **2003**, *90*, 2861-2869; (d) A. D. Andricopulo, R. A. Yunes, V. C. Filho, R. Correa, A. W. Filho, A. R. S. Santos, R. J. Nunes, *Acta Farm. Bonaerense*, **1998**, 17, 219-224.
2. (a) N. Pittala, F. Thétiot, S. Triki, K. Boukheddaden, G. Chastanet, M. Marchivie, Submitted; (b) S. Lethu, J. Dubois, *Eur. J. Org. Chem.*, **2011**, 3920-3931; (c) P. G. Baraldi, F. Fruttarolo, M. A.Tabrizi, D. Preti, R. Romagnoli, H. El-Kashef, A. Moorman, K. Varani, S. Stefania Gessi, S. Merighi, P.A. Borea, *J. Med. Chem.*, **2003**, *46*, 1229-1241.
3. G. M. Sheldrick, *Acta Cryst*. **2008**, *A64*, 112.